Clustering of Oxygen Vacancies at CeO₂(111): Critical Role of Hydroxyls

Xin-Ping Wu and Xue-Qing Gong

Key Laboratory for Advanced Materials, Centre for Computational Chemistry and Research Institute of Industrial Catalysis, East China University of Science and Technology, Shanghai 200237, People's Republic of China (Received 19 November 2015; revised manuscript received 13 December 2015; published 26 February 2016)

By performing density functional theory calculations corrected by an on site Coulomb interaction, we find that the defects at the $CeO_2(111)$ surface observed by the scanning tunneling microscopy (STM) measurements of Esch *et al.* [Science 309, 752 (2005)] are not mere oxygen vacancies or fluorine impurities as suggested by Kullgren *et al.* [Phys. Rev. Lett. 112, 156102 (2014)], but actually the hydroxyl-vacancy combined species. Specifically, we show that hydroxyls play a critical role in the formation and propagation of oxygen vacancy clusters (VCs). In the presence of neighboring hydroxyls, the thermodynamically unstable VCs can be significantly stabilized, and the behaviors of oxygen vacancies become largely consistent with the STM observations. In addition to the clarification of the long term controversy on the surface defect structures of $CeO_2(111)$, the "hydroxyl-vacancy model" proposed in this work emphasizes the coexistence of hydroxyls and oxygen vacancies, especially VCs, which is important for understanding the catalytic and other physicochemical properties of reducible metal oxides.

DOI: 10.1103/PhysRevLett.116.086102

Reducible metal oxides with oxygen vacancies that can be formed and replenished facilely are often used as the substrate or even the single active component for catalysts in a wide range of catalytic redox reactions [1–4]. Intuitively, the chemical properties of such catalysts are strongly affected by the presence and configuration of oxygen vacancies, and a conspicuous example is that the specific atomic morphology and distribution of oxygen vacancies can restrict the geometry and mobility of the supported noble-metal nanoparticles, giving rise to a unique catalytic performance and improved stability against sintering [5,6]. It then promotes the identification of the oxygen vacancy structures of such oxides at the atomic level [7–9]. Scanning tunneling microscopy (STM) and atomic force microscopy (AFM) are now among the most reliable and frequently used techniques for the direct probe of surface morphologies as well as the atomic structures of various defects including oxygen vacancies [7–10].

Ceria (CeO₂), as a particular case of reducible metal oxides, exposes the highly active surface lattice oxygen and is rich with oxygen vacancies, bringing extraordinary catalytic activities in broad applications [11–13]. Over the past twenty years, atomic-resolution STM and AFM studies have been intensively conducted to image the surface defect structures of the thermodynamically most stable (111) facet of CeO_2 [8–10,14–19]. In one pioneering work, Esch *et al.* [8] conducted STM measurements at a negative bias voltage (–3 V) to probe the surface oxygen ions through imaging the occupied states of O 2p on the surface. They found that isolated (top-)surface and subsurface oxygen vacancies (denoted as SV and SSV, respectively) with similar concentrations dominate the $CeO_2(111)$ surface after a short annealing, and abundant linear surface oxygen vacancy

clusters (LSVCs) and many triangular surface oxygen vacancy trimers (TSVTs) appear as the result of a prolonged annealing. Interestingly, they also found that only one type of TSVT, which centered on a subsurface oxygen (TSVT 1), can be observed; by contrast, the other type of TSVT that centered on a Ce ion (TSVT 2) never occurred. Oxygen vacancies and vacancy clusters have also been located in other STM and AFM studies [15–17], and detailed understanding of these results became highly demanded. However, follow-up theoretical studies using density functional theory (DFT) calculations reached a consistent conclusion that the clustering of the surface oxygen vacancies is thermodynamically *unfavorable* [20,21], which brings a controversy to the origin of this phenomenon.

Recently, Kullgren et al. proposed that the surface oxygen defects observed in the STM measurements by Esch et al. were actually fluorine impurities. This conclusion was obtained based on the following facts: (i) considerable amounts of the fluorine impurities may exist in the commercial CeO₂ single crystal samples used in the experimental studies, (ii) the simulated filled-state STM images of the surface oxygen vacancy and doped fluorine impurity are indistinguishable, and (iii) some behaviors of fluorine impurities such as their preference for pairing are consistent with the experimental observations [22]. However, we noticed that this work only calculated the energetics of the formation of the impurity dimer, which is not large enough to clarify the key STM observations of the extended defects such as the preference for linear defects in contrast to triangular ones and the missing of TSVT 2 type defects. Therefore, in this Letter, we first intend to further verify the behaviors of the fluorine impurities at CeO₂(111) by calculating the surface energetics with a high coverage of

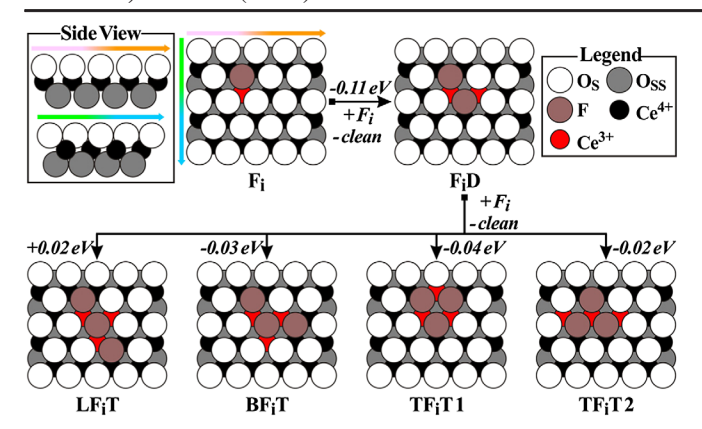


FIG. 1. Calculated energetics for the structural evolution of the clustering of fluorine impurities at $CeO_2(111)$. All of the structures are depicted in schematic plan views from the side and top. O_S and O_{SS} represent the surface and subsurface oxygen, respectively. Clean denotes the clean $CeO_2(111)$ surface.

doped fluorine. We will show that the presence of such fluorine impurities may not explain all of the experimental observations. We then present our new model, in which hydroxyls are shown to have a decisive role on the energetics and morphologies of the oxygen vacancy clusters.

Our DFT calculations employed the periodic slab model of $CeO_2(111)$ which was extended at a (4×4) surface cell and contains four O-Ce-O trilayers. We performed spin-polarized calculations by using the Perdew-Burke-Ernzerhof (PBE) functional [23] with the Hubbard U correction (DFT + U) [24]. The effective U value of 5.0 eV was applied to the localized Ce 4f states to better describe the electronic and atomic structures of ceria [25–29]. More calculation details can be found in the Supplemental Material [30].

When substituting a divalent surface oxygen for a monovalent fluorine, there occurs one excess electron that prefers to localize on the nearest neighbor Ce ion $(F_i, see$ Fig. 1) [22]. We also located the most stable configurations of the fluorine impurity dimer (F_iD) as well as the trimers (F_iT) which take the linear, bent, and two triangular configurations (denoted as LF_iT, BF_iT, TF_iT 1, and TF_iT 2, respectively), and determined the energetics for the structural evolution of the clustering of the fluorine impurities at $CeO_2(111)$ (Fig. 1). We found that the formation of an impurity dimer from two isolated impurities is thermodynamically favorable with a calculated binding energy of 0.11 eV, which is very close to the value of 0.08 eV reported by Kullgren et al. [22]. However, for the formations of the impurity trimers from one dimer and one monomer, the calculated binding energies are essentially identical and rather small (-0.02-+0.04 eV). It also indicates that TF_iT 2, which centers on a Ce ion, is slightly favored on the surface, and the linear configurations of fluorine impurities will not dominate the surface, which is largely conflicted with the STM observations [8].

The search for the legitimate "vacancy model" then continues. In this work, we first constructed reduced

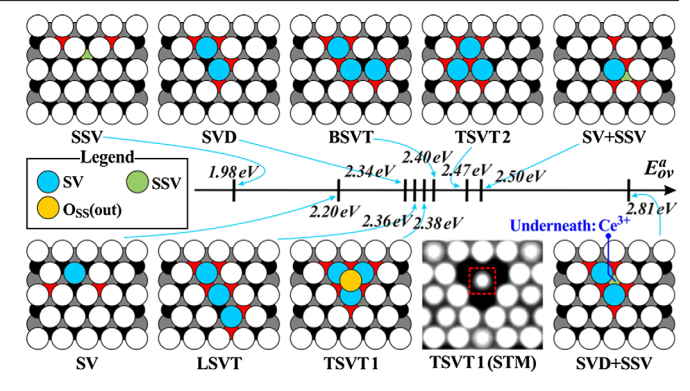


FIG. 2. Illustrative diagrams and calculated averaged oxygen vacancy formation energies of reduced $CeO_2(111)$ surfaces. The simulated filled-state STM image of TSVT 1 is also shown. $O_{SS}(\text{out})$ represents the subsurface oxygen, which has a nearly identical z coordinate with the surface oxygen ions due to a strong outward relaxation. "Underneath: Ce^{3+} "stands for a Ce^{3+} in the second trilayer.

CeO₂(111) surfaces with single- and multioxygen vacancies. Specifically, the surface with a SV, a SSV, a surface oxygen vacancy dimer (SVD), one surface oxygen vacancy plus one nearest subsurface oxygen vacancy (SV + SSV), a linear and a bent surface oxygen vacancy trimer (LSVT/BSVT), a triangular surface oxygen vacancy trimer that centers on a subsurface oxygen (TSVT 1) or on a Ce ion (TSVT 2), and a SVD plus one nearest subsurface oxygen vacancy (SVD + SSV) were constructed (Fig. 2). Among them, the SV + SSV and SVD + SSV configurations were proposed by Esch et al. to explain the linear surface defects they observed. We also located the most favorable Ce3+ distributions for each configuration. For example, after the formation of a SV or SSV, the two electrons are well localized on the two second nearest Ce cations [36,37]. To estimate the stability of the oxygen vacancy clusters (VCs), we used the averaged oxygen vacancy formation energy (E_{ov}^a) :

$$E_{ov}^a = \left[\frac{n}{2}E_{O_2} + E_{\text{surf}}^n - E_{\text{surf}}^{\text{stoi}}\right]/n,$$

where E_{O_2} , $E_{\rm surf}^n$, and $E_{\rm surf}^{\rm stoi}$ are the calculated total energies of an O_2 molecule, the surface with n oxygen vacancies, and the stoichiometric surface, respectively. It can be seen from the calculation results in Fig. 2 that all VCs have higher averaged oxygen vacancy formation energies than an isolated SV and SSV, indicating that repulsive interactions exist between oxygen vacancies [38] and they prefer to stay in isolation, which is indeed consistent with the previous theoretical predictions but largely inconsistent with the STM observations [20,21]. However, we still noticed one good agreement between the experimental and theoretical results; i.e., TSVT 1 is much more stable (by $0.27 \, {\rm eV}$) than TSVT 2. This could be simply due to the fact that the Ce cation in the center of TSVT 2 has a coordination number of four only, while those in TSVT

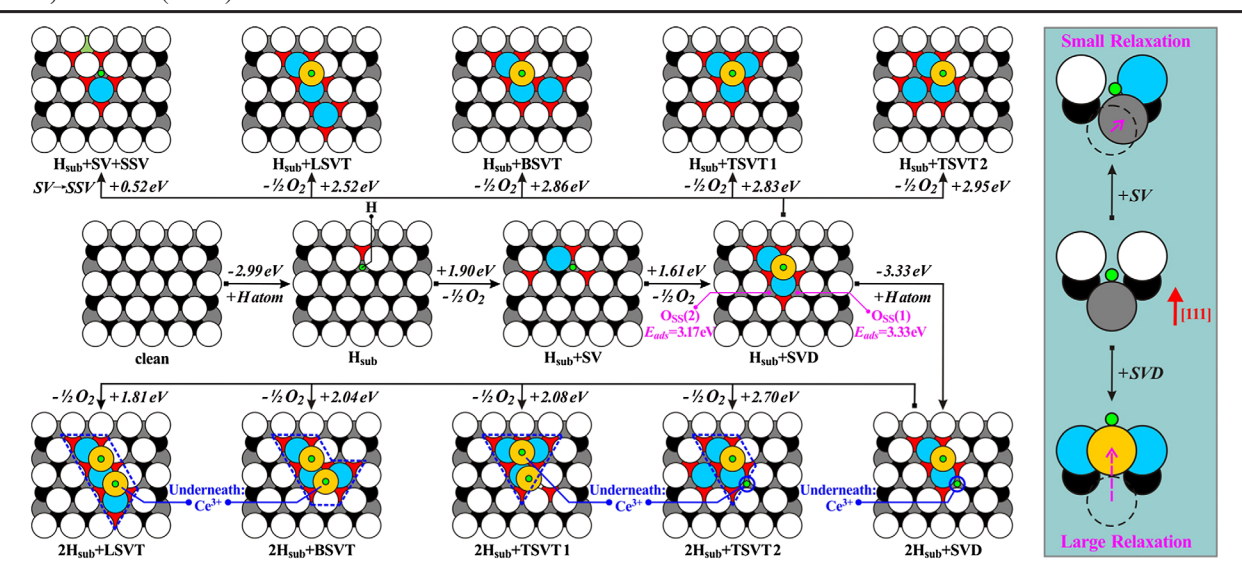


FIG. 3. Left panel: Calculated energetics for the structural evolution of the growth of surface VCs at a hydroxylated $CeO_2(111)$. The oxygen vacancy diffusion (SV \rightarrow SSV) of the $H_{sub} + SVD$ is also shown. Vacancy spaces are indicated by dashed blue polygons. Hydrogen adsorption energies for the surrounding O_{SS} ions in the $H_{sub} + SVD$ local structure are also labeled. Right panel: Schematic side view for the relaxation of the subsurface hydroxyl after the formation of one or two nearest neighbor SVs. (see Supplemental Material [30] for the detailed structural information, Figs. S2 and S3).

1 have coordination numbers of at least five. Not surprisingly, without such a prominent structural difference, the two triangular cases of fluorine impurities have a nearly identical stability. However, we found that the simulated STM image of TSVT 1 is somewhat different with the experimental one, with a characteristic bright spot (highlighted by a red dashed box) existing in the center of the triangular dark area, which is due to the strong outward relaxation of the subsurface oxygen. We then speculated that some species may stabilize the VCs, which may also influence their appearances in STM images.

In fact, we recognize the universal existence of various hydrogen sources (e.g., water) introduced during the sample preparation [11,39-41], leading to the formation of surface and bulk hydroxyls [42,43], which can be hardly eliminated even under ultrahigh vacuum conditions. Moreover, the annealing treatment of the CeO₂ samples at high temperatures may also induce the bulk infiltration of the surface proton [44-46], which further increases the amount of bulk hydroxyls. It then suggests the importance to study the role of such hydroxyls in the formation of surface VCs. Subsurface hydroxyls may occur as the result of the facile diffusion of H in bulk CeO₂ [47] and are most likely to play such an important role since they are the close neighbors to surface VCs, and unlike the surface hydroxyls that points the H away from the surface plane, they may have obvious lateral interactions with the VCs. It can be seen from the left panel of Fig. 3 that the formation of a SV that directly neighbors to the subsurface hydroxyl is significantly more favorable than the original one (1.90 vs 2.20 eV). In addition, further formation of another SV for the occurrence of a SVD is even more facile, with an oxygen vacancy formation energy of 1.61 eV only,

indicating that the isolated vacancies tend to form a vacancy dimer very strongly in the presence of a subsurface hydroxyl. Detailed analyses showed that structural relaxation of the subsurface hydroxyl assists the formation of SV and then the SVD; in the formation of the first SV, the subsurface hydroxyl slightly moves toward the newly formed vacancy, while it has a strong outward relaxation and splits the vacancy dimer when the SVD forms (see the right panel of Fig. 3). In other words, vacancies can provide spaces for *neighboring* hydroxyls to relax, and such stabilization effect from the coexisted oxygen vacancies and subsurface hydroxyls further confirms the role of the subsurface hydroxyls in the surface VCs formation (see Supplemental Material [30] for details, Fig. S1). It also reflects that such a stabilization effect can readily overcome the "repulsive interactions" between neighboring vacancies, which are caused by counteracting vacancy-induced lattice relaxation and Ce³⁺ with a large size [38,48]. In addition, in line with the observations of Esch et al., such a SVD is stable and immobile because the diffusion of a SV in a SVD to the neighboring subsurface site (SV \rightarrow SSV) is thermodynamically unfavorable with an energy increase of 0.52 eV, simply due to the fact that such a diffusion may suppress the outward relaxation of the subsurface hydroxyl.

However, our calculation results show that the formation of various different surface oxygen vacancy trimers (SVTs) evolving from such a SVD is rather difficult with calculated formation energies for the extra vacancy of more than 2.5 eV. This could be because that formation of such an extra vacancy beside the SVD cannot be benefited from further relaxation of the deeply relaxed subsurface hydroxyl. At the same time, we found that the $H_{\text{sub}}+SVD$ combined species can actually attract one proton from

TABLE I. The calculated formation energies (in eV) of the newly developed oxygen vacancy in the growing oxygen vacancies on the clean and hydroxylated surfaces.

	clean → SV	SV → SVD	SVD → LSVT	SVD → BSVT	SVD → TSVT 1	$\begin{array}{c} \text{SVD} \rightarrow \\ \text{TSVT 2} \end{array}$	clean → SSV	SSV → SSVD
Clean	2.20	2.48	2.40	2.52	2.46	2.73	1.98	2.38
Hydroxylated	1.90	1.61	1.81	2.04	2.08	2.70	1.93	1.88

another bulk hydroxyl to adsorb at its surrounding subsurface O (O_{SS}) ions ($E_{\rm ads}=3.33$ eV at the O_{SS}(1), Fig. 3) to form a $2H_{sub} + SVD$ species ($E_{ads} = 2.99$ eV at O_{SS} of clean CeO₂(111), see Supplemental Material [30] for the calculation details). This new subsurface hydroxyl has a strong tendency for further relaxation and can therefore favor the occurrence of a new SV, leading to the formation of SVTs. Specifically, the formation of an oxygen vacancy for the SVD \rightarrow LSVT evolution is the most favorable to occur and costs 1.81 eV (Fig. 3), which is also smaller than that of an isolated SV (1.90 eV). Then, longer LSVCs [8] can be expected to readily occur by such a two-step mechanism containing the H attraction and oxygen vacancy growth, though the explicit simulations of the alternate occurrences of more subsurface OHs and surface oxygen vacancies may need much larger surface cells.

It should be noted that formations of the BSVT and TSVT 1 from the SVD are competitive with each other, but more difficult than that of the LSVT (Fig. 3). Interestingly, evolution of a SVD to a TSVT 2 gives a rather high oxygen vacancy formation energy of 2.70 eV, which in fact prevents the formation of TSVT 2 (Fig. 3). This is because the third SV in a TSVT 2 stays away from the original vacancy area of a SVD by one surface Ce cation, which then restricts the relaxation of the second subsurface hydroxyl; by contrast, in other SVTs, the three SVs merge to give even more space for the hydroxyl relaxation (see dashed blue polygons in bottom of Fig. 3). The calculated formation energies of the newly developed oxygen vacancy in the growing oxygen vacancies on the clean and hydroxylated surfaces are summarized in Table I. It clearly shows that the growth of VCs becomes favorable with the existence of subsurface hydroxyls, and particularly, the LSVT/BSVT should be the most popular to occur, followed by the TSVT 1 type VCs, while the TSVT 2 should be hard to be observed. These results are indeed well consistent with the STM observations of Esch et al.

It needs to be mentioned that the results listed in the last two columns of Table I also show that SSVs can be slightly stabilized by neighboring bulk hydroxyls, which located in the third oxygen layer, with 0.05 eV. In addition, the calculated formation energies of SSV with and without hydroxyl (1.98 and 1.93 eV) are both close to that of a SV stabilized by the hydroxyl (1.90 eV), indicating the similar concentration of them as observed by Esch *et al.* Moreover, with the assistance of a hydroxyl, the formation of a subsurface oxygen vacancy dimer (SSVD) is slightly favored with respect to isolated SSVs (1.88 vs 1.98 eV),

which implies the tendency toward clustering (see Supplemental Material [30] for structural information, Fig. S4). Accordingly, the stabilization effect from the strong relaxation of a hydroxyl toward the vacancy space may also work in the formation of subsurface VCs, suggesting the wide applicability of this model. However, it also needs to be noted that the calculated formation energy of the newly developed SSV in the SSVD is actually much larger than that in the SVD (1.88 vs 1.61 eV), suggesting that the bulk hydroxyls may essentially be involved in the formation of surface VCs while arrangements of subsurface O vacancies separated by $\sqrt{3}$ or 2 times the closest possible distance between vacancies may still occur [10,19].

Finally, we simulated the filled-state STM images (bias -3 V) of the three most stable SVTs that involve two subsurface hydroxyls. Surprisingly, the outward relaxed subsurface hydroxyls cannot be seen in the simulated STM images though they are also in the surface plane (top panel, Fig. 4) [22,49]. From the calculated local density of states (LDOS) shown in the bottom panel of Fig. 4, we can see that the occupied 2p states of the $O_{SS}(out)$ of the hydroxyl largely lie at the energy levels of \sim 3 eV lower than the Fermi level, while a normal O_S distributes most of its states within the range of -3--1.7 eV. Accordingly, the "surface" hydroxyls cannot be detected in the STM measurement with a bias voltage at or higher than -3 V.

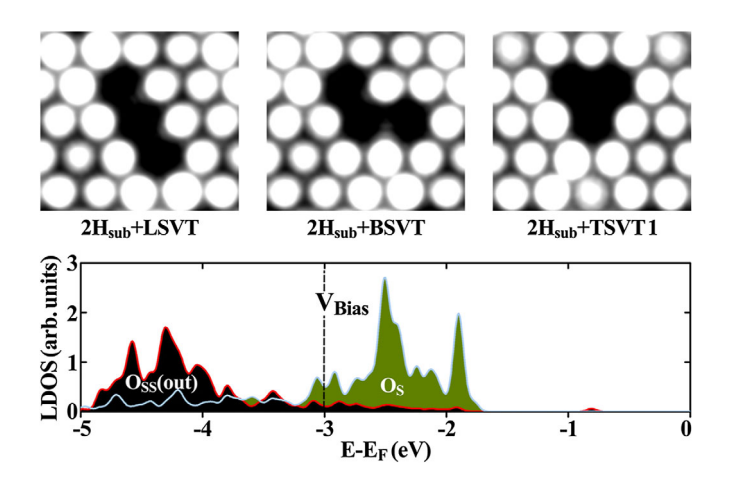


FIG. 4. Up panel: Simulated filled-state STM images (bias -3 V) of the three most stable SVTs that involve two outward relaxed subsurface hydroxyls. Bottom panel: Calculated local density of states (LDOS) of two typical oxygen ions, i.e., a normal O_S and an O_{SS} (out) of the subsurface hydroxyl, in the $2H_{sub} + LSVT$ structure.

Most importantly, the simulated STM images are now quite similar to the experimental ones [8], again proving the validity of the "hydroxyl-vacancy model".

In summary, we propose the "hydroxyl-vacancy model" in this Letter that shows a surprisingly high consistence with the experimental observations regarding the energetics and appearances of the surface defects of CeO₂(111), thus clarifying the long term controversy on the clustering of oxygen vacancies at CeO₂(111). Specifically, we determined the critical role of hydroxyls in the formation and propagation of VCs. Our results suggest that oxygen vacancies, especially VCs, may in fact prefer to coexist with hydroxyls due to their mutual stabilization effect, thereby bringing important atomic structural information for studying the surface science of a reduced CeO₂ as well as many other reducible metal oxides.

We are grateful for financial support from the National Natural Science Foundation of China (Grants No. 21421004, No. 21322307), "Shu Guang" project of Shanghai Municipal Education Commission and Shanghai Education Development Foundation (Grant No. 13SG30) and the Fundamental Research Funds for the Central Universities (Grant No. WD1313009). The authors also thank the computing time in the National Super Computing Center in Jinan.

- xgong@ecust.edu.cn
- [1] I. X. Green, W. Tang, M. Neurock, and J. T. Yates Jr., Science 333, 736 (2011).
- [2] M. Cargnello, V. V. T. Doan-Nguyen, T. R. Gordon, R. E. Diaz, E. A. Stach, R. J. Gorte, P. Fornasiero, and C. B. Murray, Science 341, 771 (2013).
- [3] N. J. Divins, I. Angurell, C. Escudero, V. Pérez-Dieste, and J. Llorca, Science 346, 620 (2014).
- [4] G. Vilé, B. Bridier, J. Wichert, and J. Pérez-Ramírez, *Angew. Chem., Int. Ed. Engl.* 51, 8620 (2012).
- [5] J. A. Farmer and C. T. Campbell, Science 329, 933 (2010).
- [6] N. Lopez, J. K. Nørskov, T. V. W. Janssens, A. Carlsson, A. Puig-Molina, B. S. Clausen, and J.-D. Grunwaldt, J. Catal. 225, 86 (2004).
- [7] O. Dulub, M. Batzill, S. Solovev, E. Loginova, A. Alchagirov, T. E. Madey, and U. Diebold, Science **317**, 1052 (2007).
- [8] F. Esch, S. Fabris, L. Zhou, T. Montini, C. Africh, P. Fornasiero, G. Comelli, and R. Rosei, Science 309, 752 (2005).
- [9] J.-F. Jerratsch, X. Shao, N. Nilius, H.-J. Freund, C. Popa, M. V. Ganduglia-Pirovano, A. M. Burow, and J. Sauer, Phys. Rev. Lett. 106, 246801 (2011).
- [10] S. Torbrügge, M. Reichling, A. Ishiyama, S. Morita, and Ó. Custance, Phys. Rev. Lett. 99, 056101 (2007).
- [11] A. Trovarelli, *Catalysis by Ceria and Related Materials* (Imperial College Press, London, 2002).
- [12] Q. Fu, H. Saltsburg, and M. Flytzani-Stephanopoulos, Science 301, 935 (2003).
- [13] J. A. Rodriguez, S. Ma, P. Liu, J. Hrbek, J. Evans, and M. Pérez, Science 318, 1757 (2007).

- [14] H. Nörenberg and G. A. D. Briggs, Phys. Rev. Lett. 79, 4222 (1997).
- [15] H. Nörenberg and G. A. D. Briggs, Surf. Sci. 424, L352 (1999).
- [16] K. Fukui, Y. Namai, and Y. Iwasawa, Appl. Surf. Sci. 188, 252 (2002).
- [17] Y. Namai, K. Fukui, and Y. Iwasawa, Catal. Today 85, 79 (2003).
- [18] S. Gritschneder and M. Reichling, Nanotechnology 18, 044024 (2007).
- [19] D. C. Grinter, R. Ithnin, C. L. Pang, and G. Thornton, J. Phys. Chem. C 114, 17036 (2010).
- [20] C. Zhang, A. Michaelides, D. A. King, and S. J. Jenkins, Phys. Rev. B 79, 075433 (2009).
- [21] J. C. Conesa, Catal. Today 143, 315 (2009).
- [22] J. Kullgren, M. J. Wolf, C. W. M. Castleton, P. Mitev, W. J. Briels, and K. Hermansson, Phys. Rev. Lett. **112**, 156102 (2014).
- [23] J. P. Perdew, K. Burke, and M. Ernzerhof, Phys. Rev. Lett. 77, 3865 (1996).
- [24] S. L. Dudarev, G. A. Botton, S. Y. Savrasov, C. J. Humphreys, and A. P. Sutton, Phys. Rev. B 57, 1505 (1998).
- [25] M. Nolan, S. C. Parker, and G. W. Watson, Surf. Sci. 595, 223 (2005).
- [26] J. L. F. DaSilva, M. V. Ganduglia-Pirovano, J. Sauer, V. Bayer, and G. Kresse, Phys. Rev. B 75, 045121 (2007).
- [27] C. Loschen, J. Carrasco, K. M. Neyman, and F. Illas, Phys. Rev. B 75, 035115 (2007).
- [28] C. W. M. Castleton, J. Kullgren, and K. Hermansson, J. Chem. Phys. 127, 244704 (2007).
- [29] J. P. Allen and G. W. Watson, Phys. Chem. Chem. Phys. 16, 21016 (2014).
- [30] See Supplemental Material at http://link.aps.org/supplemental/10.1103/PhysRevLett.116.086102 for computational details and complementary calculation results, which includes Refs. [8] and [31–35].
- [31] G. Kresse and J. Furthmüller, Comput. Mater. Sci. 6, 15 (1996).
- [32] G. Kresse and J. Hafner, Phys. Rev. B 49, 14251 (1994).
- [33] P. E. Blöchl, Phys. Rev. B 50, 17953 (1994).
- [34] E. A. Kummerle and G. Heger, J. Solid State Chem. 147, 485 (1999).
- [35] J. Tersoff and D. R. Hamann, Phys. Rev. B 31, 805 (1985).
- [36] M. V. Ganduglia-Pirovano, J. L. F. DaSilva, and J. Sauer, Phys. Rev. Lett. 102, 026101 (2009).
- [37] H.-Y. Li, H.-F. Wang, X.-Q. Gong, Y.-L. Guo, Y. Guo, G. Lu, and P. Hu, Phys. Rev. B 79, 193401 (2009).
- [38] G. E. Murgida and M. V. Ganduglia-Pirovano, Phys. Rev. Lett. **110**, 246101 (2013).
- [39] X. Feng, D. C. Sayle, Z. L. Wang, M. S. Paras, B. Santora, A. C. Sutorik, T. X. T. Sayle, Y. Yang, Y. Ding, X. Wang, and Y.-S. Her, Science 312, 1504 (2006).
- [40] S. Yang and L. Gao, J. Am. Chem. Soc. 128, 9330 (2006).
- [41] X. Liu, K. Zhou, L. Wang, B. Wang, and Y. Li, J. Am. Chem. Soc. 131, 3140 (2009).
- [42] K. Sohlberg, S. T. Pantelides, and S. J. Pennycook, J. Am. Chem. Soc. 123, 6609 (2001).
- [43] P. G. Lustemberg, M. V. Bosco, A. Bonivardi, H. F. Busnengo, and M. V. Ganduglia-Pirovano, J. Phys. Chem. C 119, 21452 (2015).

- [44] J. L. G. Fierro, S. Mendioroz, and A. M. Olivan, J. Colloid Interface Sci. 107, 60 (1985).
- [45] J. L. G. Fierro, J. Soria, J. Sanz, and J. M. Rojo, J. Solid State Chem. **66**, 154 (1987).
- [46] L. A. Bruce, M. Hoang, A. E. Hughes, and T. W. Turney, Appl. Catal., A **134**, 351 (1996).
- [47] X.-P. Wu, X.-Q. Gong, and G. Lu, Phys. Chem. Chem. Phys. 17, 3544 (2015).
- [48] Y. Pan, N. Nilius, H.-J. Freund, J. Paier, C. Penschke, and J. Sauer, Phys. Rev. Lett. **111**, 206101 (2013).
- [49] C. W. M. Castleton, A. Höglund, M. Göthelid, M. C. Qian, and S. Mirbt, Phys. Rev. B **88**, 045319 (2013).